

Synthesis and characterization of poly (o-methyl aniline) – MMT (Cloisite30B) nanocomposites for corrosion protection

Prasanna Kumar Sahoo¹, Dillip Kumar Behera², Matru Prasad Dash², Bijaya Kumar Parija²,
Munesh Chandra Adhikari³ and P.L.Nayak¹

¹Orissa Engineering College, Bhubaneswar-752050

² Center of Excellence of Nanoscience and Engineering, Synergy Institute of Technology, Bimpur, Phulnakhara.

³Department of Physics, F.M. University, Balasore, India

Abstract

In the present research program, the synthesis and characterization of poly(o-methyl aniline) has been carried out by blending it with MMT (Cloisite 30B). The composites were characterized by using UV-visible, SEM, and XRD studies, The conductive and corrosion resistance of the composites have also been investigated. In situ UV-vis spectroscopy of OMPANI–MMT nanocomposites indicates that electrochromic behaviour of OMPANI in the nanocomposite is retained. The larger interlayer spacing observed in X-ray diffraction studies confirms the intercalation of anilinium ions. It also shows that electro polymerization of o-methyl aniline inside the clay tactoids yielding highly stereo regular conducting OMPANI as d-spacing of OMPANI–MMT is close to that of anilinium-MMT. The electrical conductivity as well as the corrosion resistance of the nanocomposites have been investigated.

Key words: Orthomethyl aniline, polymerization. Conducting polymers, MMT, Composites

Date of Submission: 17, December, 2012  Date of Publication: 11, January 2013

I. Introduction

Generally composite materials can be defined as materials consisting of two or more components with different properties and distinct boundaries between the components. The idea of combining several components to produce a new material with new properties that are not attainable with individual components has been used intensively in the past. Correspondingly, the majority of natural materials that have emerged as a result of prolonged evolution process can be treated as composite materials [1, 2].

Nanocomposites are generally defined as composites in which the components have at least one dimension (i.e., length, width or thickness) in the size range of 1-100 nm. Nanocomposites differ from traditional composites in a sense that interesting properties can result from the complex interaction of the nanostructured heterogeneous phases. In addition, nanoscopic particles of a material differ greatly in the analogous properties from a macroscopic sample of the same material [3, 4, 5].

Conducting polymers are a class of polymer with conjugated double bonds in their backbones. They display unusually high electrical conductivity and become highly conductive only in their doped state. Due to the excellent electrical and electronic properties and plastic nature of conducting polymers, they have been proposed for application such as antistatic coating, corrosion protection, electrochromic display, sensors, light-emitting diodes, capacitors, light weight batteries and gas permeation membranes, etc. They are also believed to be promising alternatives to the environmentally hazardous chromate conventional coating. There are many published reports focusing on the design, preparation and characterization of novel organic-inorganic nanocomposites consisting of conducting polymer with various layered materials, such as FeOCl [6], MoO₃ [7-8], V₂O₅ [9] and clay minerals (montmorillonite (MMT)) [10-21]. Since then the advent of the nano-technology era, nanocomposites composed of conducting polymers and inorganic particles have aroused much interest in the scientific community. In order to improve the interesting properties possessed by conducting polymers and to generate new properties, researchers are formulating organic-inorganic hybrid materials based on conducting polymers. Layered materials, such as smectite clays (e.g., Na⁺–montmorillonite, Na⁺–MMT) attracted great research interests for the preparation of polymer–clay nanocomposite materials in the past decade, because of its small particle (<10 nm) and easy of intercalation [15]. The Na⁺–MMT, whose lamella is constructed from an octahedral alumina sheet sandwiched between two tetrahedral silica sheets, exhibits a net negative charge on the surface of layers. The cation such as Na⁺ or Ca²⁺ is absorbed on the surface to compensate the net negative

charge [16]. The increase in interlayer spacing that occurs with swelling of the Na⁺-MMT clay in water is large and enables the particles to be penetrated by relatively large size molecules [17].

Currently organophilically charged clay layers exchanged by cationic surfactants playing an important role for the intercalation [16,18]. There are a number of reports on the preparation and properties for the nanocomposite materials of PANI with various layered materials through the conventionally oxidative polymerization reactions [19–26]. In this paper, we present the synthesis and characterization of polymer(o-methyl aniline) blended with MMT (Cloisite 30 B) using radical polymerization method. The polymers were characterized by using UV-visible , XRD, SEM, methods. The conductivity measurements as well as the corrosion resistance of the composites have also been investigated.

II. Experimental

Synthesis of o-methyl polyaniline(OMPANI)- MMT nanocomposites

The nanocomposites were synthesized chemically from o-methyl aniline free anilinium-MMT dispersion in 0.3 M sulfuric solution. The 0.1 M ammonium persulfate solution was used as oxidizing agent. The polymerization was carried out at room temperature under magnetic stirring. The resulting OMPANI-MMT was filtered, washed with excess deionized water, dried in vacuum for 4 days. The final OMPANI-MMT nanocomposites were ground using a mortar and pestle for characterization.

III. Characterization Techniques

UV-visible Spectroscopy

In situ UV-Vis spectra were recorded with a Shimadzu model UV-2101 PC spectrometer. Experiments were carried out in a 1 cm path length quartz cuvette arranged with a OMPANI-MMT deposited ITO electrode that was used as working electrode, installed perpendicularly to the light path. A platinum wire was used as counter electrode. A saturated calomel electrode connected *via* a salt bridge served as reference electrode. In the reference channel of spectrometer a quartz cuvette filled with 0.5 M sulfuric acid solution containing an identical ITO glass electrode was placed. *In situ* measurements were carried out under ambient conditions.

X-ray diffraction

The powder samples of OMPANI-MMT nanocomposites were dried as before elemental analysis. X-ray diffraction measurements were carried out on a Seifert FPM/XRD7 diffractometer with Ni-filtered Cu-K α radiation ($\lambda = 0.154$ nm) operated at 40 kV and 30 mA.

Cyclic voltammetry

The deposited OMPANI-MMT gold sheet electrode was used for cyclic voltammetry measurements. All cyclic voltammograms were recorded by a custom built potentiostat connected to computer using AD/DA converter. Measurements were carried out under nitrogen atmosphere in a three-compartment cell containing 0.5 M sulfuric acid solution. Another gold sheet electrode was used as counter electrode and a saturated calomel electrode was used as reference electrode.

In situ conductivity measurements

For *in situ* conductivity measurements, a double-band gold electrode was used as working electrode as described elsewhere [41]. Another gold sheet electrode and saturated calomel electrode were used as counter and reference electrodes, respectively. Electrodeposition of OMPANI-MMT on Au double band electrode was carried out potentiostatically as described in section 2.3.1 for 2 h.

The conductivity measurements were carried out in 0.5 M sulfuric acid supporting electrolyte solution. The current flowing across the band was measured with an I/V converter with an amplification factor (F_{ac}) ranging from 10^2 to 10^6 . The film resistance R_x (ohm) is related to the measured voltage U_x and the amplification factor F_{ac} according to $R_x = (0.01 \times F_{ac}) / U_x$. Electrode potential was increased stepwise by 100 mV and after approximately 5 min the electrochemical cell was cut off from the potentiostat.

Corrosion studies

In corrosion studies, a working electrode was made of mild steel (steel C45). Chemical composition of the C45 steel (wt %): C = 0.46, Si = 0.40, Mn = 0.65, Cr = 0.40, Mo = 0.10, Ni = 0.40 and others = 0.63. It was manufactured as cylinder of 10 mm height in a way to function as disk electrode with exposed area of 1.13 cm^2 , surrounded with Teflon tape. Before using, steel electrode was first polished on sand paper of 1000 grade and then on a polishing cloth with alumina slurry ($13 \mu\text{m}$).

For deposition of OMPANI-MMT on steel electrode, a saturated calomel electrode (SCE, saturated in KCl) and sheet gold electrode were employed as reference and counter electrodes, respectively. Before

electropolymerization, steel electrode was cathodically cleaned in 0.5 M oxalic acid solution for 10 min at $E_{SCE} = -900$ mV; it was subsequently passivated in two steps, a fast potentiodynamic rise up to $E_{SCE} = 1000$ mV, followed by a potentiostatic polarization at $E_{SCE} = 700$ mV during 30 min. Electrodeposition of PANI-MMT on C45 steel electrode was carried out potentiostatically. Resulting PANI-MMT coating steel electrode was washed with deionized water. In the case of soluble PANI-DBSA, the PANIs dissolved in $CHCl_3$ were drop coated on the C45 steel discs which were previously polished with fine emery paper (P 1000) and with $\gamma-Al_2O_3$ (13 μ m).

IV. Results And Discussion

4.1. In situ UV-Vis spectroscopy

Figure 1 shows *in situ* UV-Vis spectra of OMPANI-MMT, OMPANI exhibits three electronic absorption bands at 320, 430 and ~ 800 nm which originate from the $\pi \rightarrow \pi^*$ transition, radical cations and polarons respectively. Electronic absorption spectra of OMPANI-MMT, like PANI, exhibit bands at 430 and 870 nm but the band at 320 nm could not be seen. Absorbance of the band at 430 nm reaches a maximum at $E_{SCE} = 0.20$ V which indicates higher concentration of radical cations at this applied potential. At this applied potential ($E_{SCE} = 0.20$ V) the first oxidation wave in the CV of OMPANI-MMT which corresponds to the leucoemeraldine to emeraldine transition has a maximum peak current. By shifting the electrode potential to higher values, the intensity of this band diminishes. When the applied potential is increased from $E_{SCE} = -0.20$ to 0.70, maximum positions of the band at 870 nm (polaronic transition) are shifted into the near-infrared (NIR) region and at $E_{SCE} = 0.70$ this band becomes more flattened.

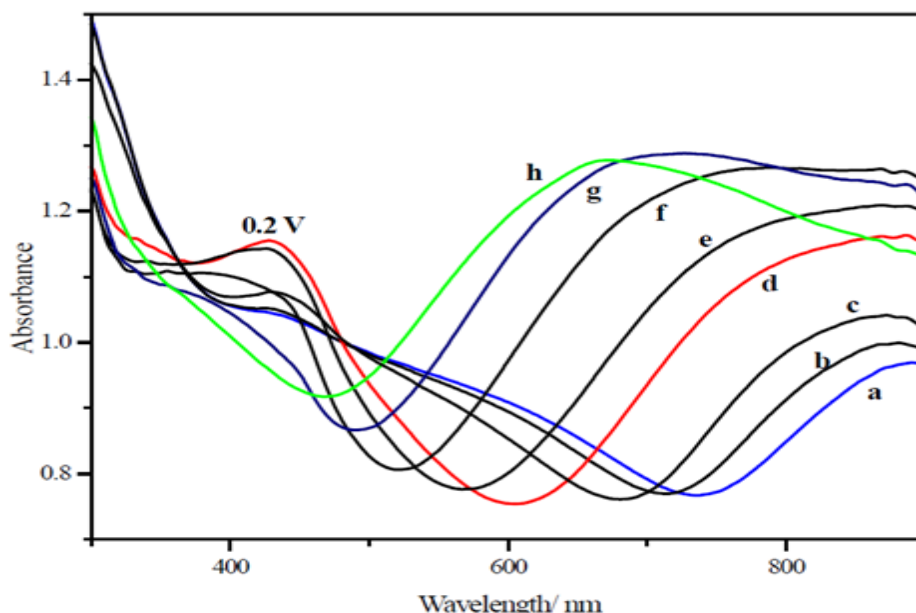


Figure1. In situ UV-Vis spectra of OMPANI-MMT recorded in 0.5 M H_2SO_4 solution at different positive going potentials (E_{SCE} / V): -0.20 (a), 0.0 (b), 0.10 (c), 0.20 (d), 0.30 (e), 0.50 (f), 0.70 (g), 0.80 (h).

4.2. SEM Studies

Morphology of OMPANI/MMT nanocomposites was studied to confirm the relationship between the electrical properties and the proposed structures of nanocomposites, SEM measurements were carried out for the same samples used for the electrical conductivity measurements. Figure 2 shows SEM micrographs of OMPANI/MMT nanocomposites with different amounts of OMPANI in the nanocomposites. From the SEM micrographs, OMPANI-MMT has a granular texture (i.e., clusters of globules as shown in Fig. 2a) and pristine MMT has a flaky texture reflecting its layered structure (Fig. 2f). It can be clearly seen in Figs. 2b–e that textures of both OMPANI-ES and pristine MMT are retained in the nanocomposites. As the OMPANI content is decreased, the characteristic granular texture of OMPANI-MMT, indicated by white arrows in Figs. 2b–d, gradually disappear and the morphology of OMPANI12 (Fig. 2e) is quite similar to that of pristine MMT.

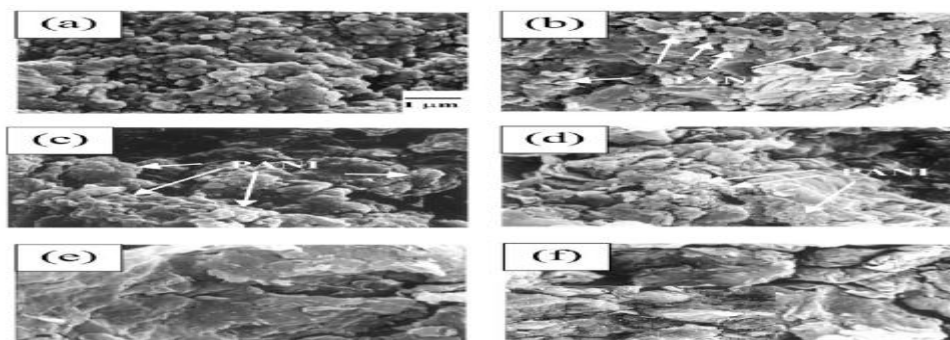


Figure 2. SEM micrographs of OMPANI/MMT nanocomposites as a function of OMPANI content: (a) OMPANI-ES, (b) OMPMN7.5 (c) OMPMN4.3 (d) OMPMN2.5 (e) OMPMN1.2 and (f) pristine MMT

4.3. X-ray diffraction

The d -spacing of the materials was calculated from the angular position 2θ of the observed peaks using the Bragg's equation: $n\lambda = 2d\sin\theta$, where λ is the wavelength of the incident X-ray beam, θ is the diffraction angle and n is an integral. Figure 3 shows X-ray diffraction patterns of OMPANI-MMT oxidized form and OMPANI-MMT reduced form (reduced form of OMPANI-MMT was obtained by applying a constant potential of $E_{SCE} = -200$ mV on a freshly synthesized oxidized sample of OMPANI-MMT for 10 min).

As shown in Figure 3 the reflection peak of the MMT sample at $2\theta = 8.8^\circ$ is shifted towards lower angles for OMPANI-MMT nanocomposites (both oxidized and reduced forms). The d -spacing of materials are 12.8 Å, 12.6 Å, 12.5 Å for anilinium-MMT, the OMPANI-MMT oxidized form, and the OMPANI-MMT reduced form, respectively. The average d -spacing of the OMPANI-MMT nanocomposites were found to be 12.55 Å, which is little bit smaller than that of anilinium-MMT. Such a smaller d -spacing for OMPANI-MMT may be due to the higher stereo regularity of OMPANI staked inside clay layers than that of anilinium ions staked inside clay layers.

Due to the insertion of OMPANI, d -spacing is expanded from 10 to 12.55 Å, that is increased by 2.55 Å. Generally, in the case of OMPANI-MMT nanocomposites, the d -spacing is expanded in the range of 0.7 to 6.0 Å [10, 11, 16, 39, 78, 79, 80]. Thus, the expansion in the d -spacing observed in this study is comparable to the data reported by other groups [41, 42]. The diffraction peak of MMT in Figure 3 is broader than with OMPANI-MMT whereas the peak anilinium-MMT is intense and sharp. The sharpness of the peaks can be influenced by crystallinity or clay-layer stacking order. Thus the broader peak of MMT indicates less crystallinity and order of clay-layer stacking than the other samples.

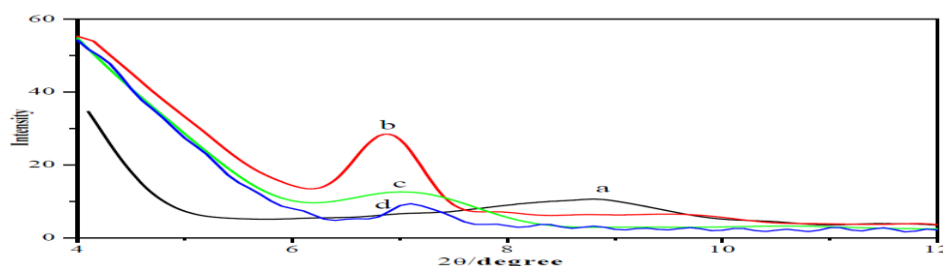


Figure 3. X-ray diffraction patterns of MMT (a), OMPANI-MMT (b), oxidized form (c) and reduced form of OMPANI-MMT (d) synthesized by electrochemical method

4.4. Cyclic voltammetry

Cyclic voltammograms (CVs) of OMPANI-MMT nanocomposites, deposited on a gold electrode, were recorded in an aqueous solution of 0.5 M sulfuric solution with different thickness as obtained after different times of electropolymerization of the OMPANI-MMT films (Figure 4). CVs of OMPANI exhibit two pairs of redox waves with the first one observed at $E_{SCE} = 200$ mV indicating the transformation of leucoemeraldine form to conducting emeraldine form and the second one at $E_{SCE} = 810$ mV which is due to the conversion of emeraldine into the pernigraniline form. A pair of humps in the region of $E_{SCE} = 0.30$ to 0.50 V has been assigned to over oxidation products. The shape of the CVs of OMPANI-MMT is similar to those of PANI. This indicates that clay layers do not influence the electrochemical properties of PANI nor does the intercalation

favour a polymer with different properties (such as e.g., molecular weight) as could evidenced with this electrochemical technique. There is only a minor shift of the reduction peak associated with the pernigraniline-emeraldine transition which might indicate some not yet understood interaction between PANI and MMT.

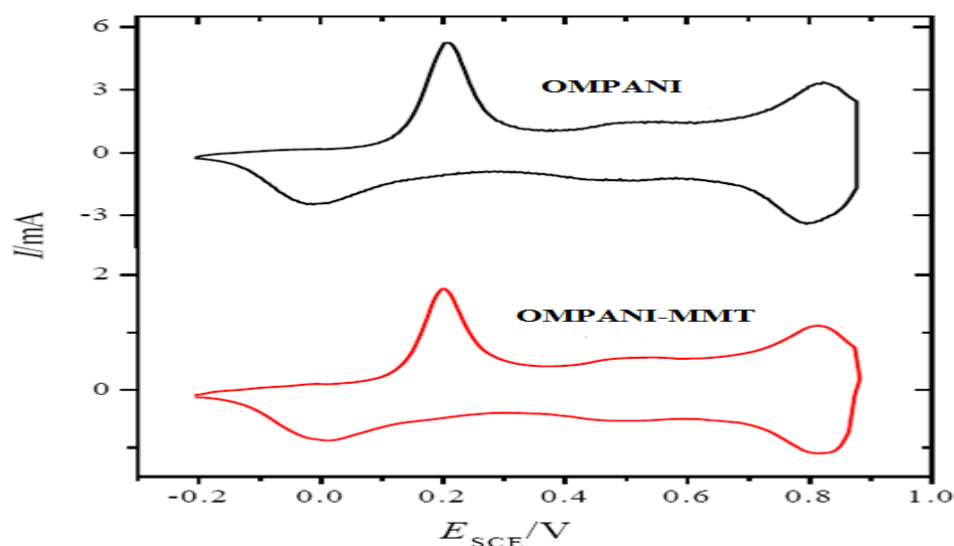


Figure.4 Cyclic voltammogram of OMPANI and OMPANI-MMT nanocomposites in 0.5 M H₂SO₄ at scan rate of 100 mV s⁻¹.

4.5. In situ conductivity measurements

Resistance values of OMPANI and OMPANI-MMT deposited at $E_{SCE} = 700$ mV were measured in an aqueous solution of 0.5 M H₂SO₄ in the range of $-0.20 < E_{SCE} < 0.9$ 0V in the anodic direction and then in the reverse cathodic direction. The $\log R$ values of both PANI and PANI-MMT against the applied electrode potential are displayed in Figure 20. Two transitions can be observed in the resistivities of both PANI and PANI-MMT. The first transition appears at around $E_{SCE} = 0$ V where the resistivity values start to decrease and the second transition appears at around $E_{SCE} = 0.60$ V where again the resistivity begins to increase. Thus in the potential range of $E_{SCE} = 0.0$ to 0.60 V, OMPANI as well as OMPANI-MMT is highly conducting, this is the potential range where PANI is in the emeraldine state. When the potential sweep direction was reversed from $E_{SCE} = 0.90$ to -0.20 V, almost similar trends were observed, however, the conductivities are lower than in the anodic sweep. This loss of *in situ* conductivity in the reverse cathodic sweep was attributed to partial degradation of PANI at $E_{SCE} = 0.90$ V. The apparent resistivity of PANI-MMT is higher than that of PANI. In the absence of data enabling the conversion of resistivities into specific resistivities a quantitative comparison is impossible. The slightly smaller relative change of resistivity in case of the nanocomposite may be due to the high fraction (90 %) of inert MMT.

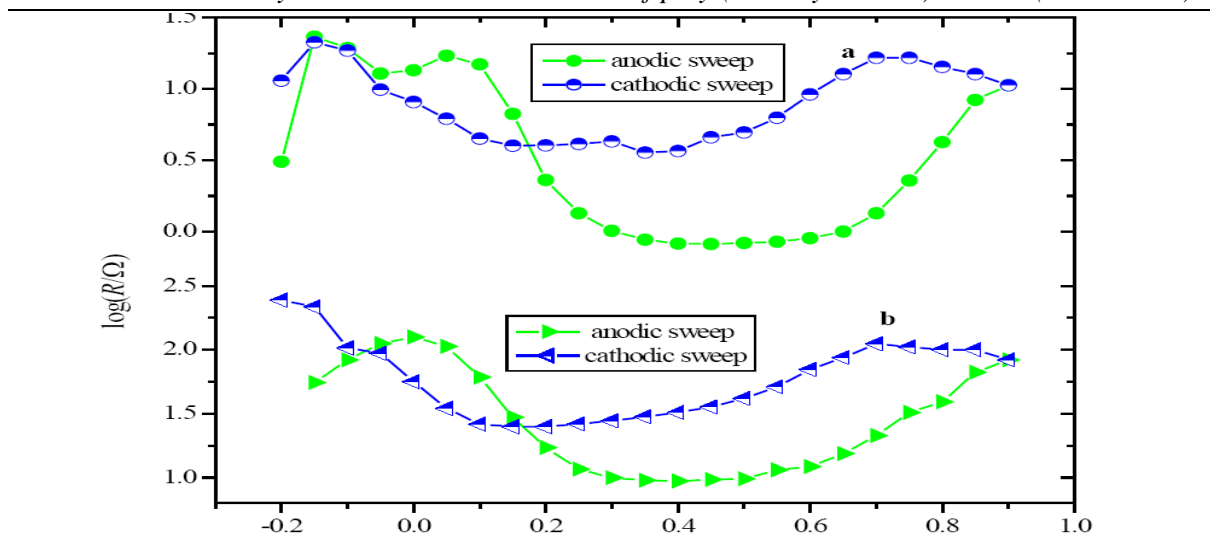


Figure 5. Plot of $\log(R)$ versus applied electrode potential for (a) OMPANI and (b) OMPANI-MMT in an aqueous solution of 0.5 M sulphuric acid.

4.6. Polarization measurements

The corrosion potential (E_{corr}) and corrosion current density (i_{corr}) can be obtained by polarization measurements. The equilibrium open circuit potential (OCP) of an electrode can be considered as E_{corr} . Corresponding to E_{corr} is i_{corr} which is proportional to corrosion rate (C_R) as shown in the equation 21 and has inverse relation with polarization resistance (R_p) of electrode as shown in equation 22 (rearrangement of Stern-Geary equation). The values of E_{corr} , i_{corr} and Tafel slopes (anodic slope b_a and cathodic slope b_c) can be obtained by extrapolation from Tafel plots. Using equation 21 and equation 22, the value of R_p and C_R of electrode can be easily determined

$$i_{\text{corr}} = \frac{C_R \cdot A \cdot d}{0.129 \cdot (EW)}$$

Where i_{corr} is corrosion current density measured in $\mu\text{A cm}^{-2}$, C_R is corrosion rate measured in millinch per year (MPY), d is density of material measured in g cm^{-3} , EW is equivalent weight of corroded metal measured in g equivalent

$$i_{\text{corr}} = \frac{b_a \cdot b_c}{2.303(b_a + b_c)} \cdot \frac{1}{R_p \cdot A}$$

Figure 6. shows Tafel plots of bare, passivated and PANI-MMT coated C45 steel electrodes. The values of E_{corr} , i_{corr} , b_a , R_p and C_R of bare, passivated and PANI-MMT coated C45 steel electrodes are calculated and shown in Table 4. For passivated C45 steel, E_{corr} is negatively shifted by 15 mV compared to bare C45 steel. This shift showed cathodic protection of passive layer. However, C_R did not decrease significantly. The corrosion potential of OMPANI-MMT coated C45 steel electrode is positively shifted by 51 mV compared to the bare C45 steel electrode. The shift of corrosion potential indicated that OMPANI-MMT coating depressed the anodic current of the corrosion reaction. The increase of corrosion potential is an indication of anodic protection by PANI-MMT. As shown in the Table 4, the corrosion rate was significantly reduced for PANI-MMT coated C45 steel as compared to the bare C45 steel electrode.

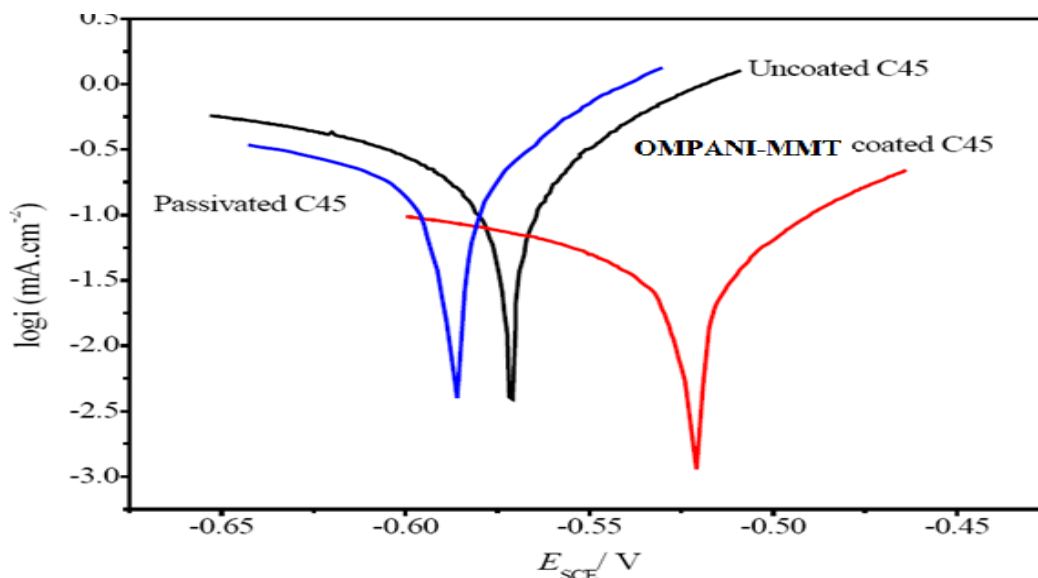


Figure 6, Tafel plot of uncoated, passivated and PANI-MMT coated C45 steel electrode in 3.5 % NaCl solution.

The polarization resistance R_p calculated from polarization measurements is in good agreement with R_{CT} value calculated from impedance measurements. The agreement between polarization resistance R_p (i.e. the slope of the current density versus electrode potential curve) and the sum of all Ohmic components in the electrode impedance deduced from impedance measurements at the same electrode potential is expected, because at frequency zero the sum of all Ohmic components of impedance is equal to said slope. The relatively small contribution of the film resistance R_F and solution resistance R_S results in a fairly good agreement between R_p and R_{CT} in the present case.

Conclusion

This piece of research work describes a new synthesis of novel composite materials based on montmorillonite (MMT) clay (Cloisite 30 B) and intrinsically conducting poly(o-methylaniline (PMPANI). OMPANI was successfully incorporated into MMT galleries to form OMPANI–MMT nanocomposites. Electropolymerization of anilinium ions which are intercalated inside the clay layers have been carried out at a constant applied potential. The synthetic conditions have been optimized taking into account the effect of concentration of aniline, magnetic stirring and potential cycling. The resulting organic-inorganic hybrid material, OMPANI-MMT has been characterized by various physicochemical techniques. Formation of OMPANI inside the clay tactoid has been confirmed by the expansion of inter layer distance of MMT as revealed by X-ray diffraction studies. Relatively lower interlayer expansion for OMPANI-MMT than that of anilinium-MMT indicates the higher stereoregularity in OMPANI-MMT which has strong influence on electrical properties of nanocomposites. Infrared spectroscopy studies reveal the presence of physicochemical interaction, probably hydrogen bonding, between clay and poly(o-OMPANI). Cyclic voltammetry studies indicate that presence of electroinactive clay does not influence the electrochemical activity of PANI. Electrochromic behaviour of OMPANI-MMT nanocomposites have been studied using *in situ* UV-Vis spectroscopy which reveals that electrochromism of OMPANI in the composite material has been retained. One of the main technological applications of conducting polymers, particularly OMPANI, is in the area of corrosion protection of active metals. OMPANI-MMT nanocomposites synthesized using the present method and a chemically synthesized OMPANI which is soluble in organic solvents have been used to protect steel surface against corrosion. Corrosion studies have been performed using electrochemical impedance measurements.

Acknowledgement:

Authors are thankful to Sri.Binod Dash,CMT ,Synergy Group of Institutions for his kind cooperation and support throughout the research work.

References

- [1]. V. V. Vasiliev, E. V. Morozov, In *Mechanics and analysis of Composite Materials*, 1st ed., Elsevier, Netherlands, 2001.
- [2]. R. M. Jones, In *Mechanics of Composite Materials*, 2nd ed., Taylor & Frances, USA, 2001.
- [3]. P. M. Ajayan, L. S. Schadler, P. V. Braun, In *Nanocomposite Science and Technology*, Wiley-VCH, Weinheim, 2003.
- [4]. Q. H. Zeng, D. Z. Wang, A. B. Yu, G. Q. Lu, *Nanotechnology* 13 (2002) 549.
- [5]. Y. Zhu, In *Synthesis, characterization and corrosion performance of polyaniline montmorillonite clay nanocomposites*, PhD thesis 2003.
- [6]. C. G. Wu, D. C. DeGoot, H. O. Marcy, J. L. Schindler, C. R. Kannewurf, T. Bakas, V. Papaefthymiou, W. Hirpo, J. P. Yesinowski, Y. J. Liu, M. G. Kanatzidis, *J. Am. Chem. Soc.* 117 (1995) 9229.
- [7]. G. R. Goward, T. A. Kerr, W. P. Power, L. F. Nazar, *Adv. Mater.* 10 (1998) 449.
- [8]. T. A. Kerr, H. Wu, L. F. Nazar, *Chem. Mater.* 8 (1996) 2005.
- [9]. M. G. Kanatzidis, C.G. Wu, H. O. Marcy, C. R. Kannewurf, *J. Am. Chem. Soc.* 111 (1989) 4139.
- [10]. G. M. do Nascimento, V. R. L. Constantino, R. Landers, M. L. A. Temperini, *Macromolecules* 37 (2004) 9373.
- [11]. W. M. de Azevedo, M. O. E. Schwartzl, G. C. do Nascimento, E. F. J. da Silva, *Phys. Stat. Sol. (C)* 1 (2004) S249.
- [12]. B. H. Kim, J. H. Jung, J. W. Kim, H. J. Choi, J. Joo, *Synth. Met.* 117 (2001) 115.
- [13]. T. Lan, P. D. Kaviratna, T. J. Pinnavaia, *Chem. Mater.* 6 (1994) 573.
- [14]. H. L. Tyan, Y. C. Liu, K. H. Wei, *Chem. Mater.* 11 (1999) 1942.
- [15]. K. H. Chen, S. M. Yang, *Synth. Met.* 135–136 (2003) 151.
- [16]. J. W. Kim, S. G. Kim, H. J. Choi, M. S. Jhon, *Macromol. Rapid Commun.* 20 (1999) 450.
- [17]. M. Pichowicz, R. Mokaya, *Chem. Mater.* 16 (2004) 263.
- [18]. T. Lan, P. D. Kaviratna, T. J. Pinnavaia, *Chem. Mater.* 7 (1995) 2144.
- [19]. G. M. do Nascimento, V. R. L. Constantino, M. L. A. Temperini, *Macromolecules* 35 (2002) 7535.
- [20]. H. L. Fisch, B. Xi, Y. Quin, M. Rafailovich, N. L. Yang, X. Yan, *High perform. Polym.* 12 (2000) 543.
- [21]. H. J. Choi, J. W. Kim, M. H. Noh, D. C. Lee, M. S. Suh, M. J. Shin, M. S. Jhon, *J. Mater. Sci. Lett.* 18 (1999) 1505.
- [22]. P. S. Rao, D. N. Sathyanarayana, In *Advanced Functional Molecules and Polymers*, H. S. Nalwa (ed.), Gordon & Breach, Tokyo, 2001.
- [23]. J. C. Chiang, A. G. McDiarmid, *Synth. Met.* 13 (1986) 193.
- [24]. E. T. Kang, K. G. Neoha, K. L. Tan, *Prog. Polym. Sci.* 23 (1998) 277.
- [25]. S. Shreepathi, R. Holze, *Chem. Mater.* 17 (2005) 4078.
- [26]. Y. Furukawa, F. Ueda, Y. Hyodo, I. Harada, T. Nakajima, T. Kawagoe, *Macromolecules* 21 (1998) 1297.
- [27]. K. G. Conroy, C. B. Breslin, *Electrochim. Acta* 48 (2003) 721.
- [28]. J. E. Mark, In *Polymer data Handbook*, Oxford University, 1999.
- [29]. E. M. Genies, A. Boyle, M. Lapkowski, C. Tsintavis, *Synth. Met.* 36 (1990) 139.
- [30]. M. M. Popovic, B. N. Grgur, V. B. Miskovic-Stankovic, *Prog. Org. Coat.* 52 (2005) 359.
- [31]. A. T. Özyilmaz, *Prog. Org. Coat.* 54 (2005) 127.
- [32]. G. Bereket, E. Hür, Y. Sahin, *Prog. Org. Coat.* 54 (2005) 63.
- [33]. A. Talo, P. Pasiniemi, O. Forsen, S. Yläsaari, *Synth. Met.* 85 (1997) 1333.
- [34]. B. Wessling, *Synth. Met.* 85 (1997) 1313[35] W. K. Lu, R. L. Elsenbaumer, B. Wessling, *Synth. Met.* 71 (1995) 2163.
- [35]. A. J. Dominis, G. M. Spinks, G. G. Wallace, *Prog. Org. Coat.* 48 (2003) 43.
- [36]. D. E. Tallman, G. Spinks, A. Dominis, G. G. Wallace, *J. Solid State Electrochem.* 6 (2002) 73.
- [37]. J. Stejskal, R. G. Gilbert, *Pure Appl. Chem.* 74 (2002) 857.
- [38]. B. Feng, Y. Su, J. Song, K. Kong, *J. Mater. Sci. Lett.* 20 (2001) 293.
- [39]. M. Kato, A. Usuki, In *Polymer-Clay Nanocomposites*, John Wiley & Sons, New York, 2000, p. 98.
- [40]. S. Yoshimoto, F. Ohashi, Y. Ohnishi, T. Nonami, *Synth. Met.* 145 (2004) 265.